# An M-channel Directional Filter Bank Compatible with the Contourlet and Shearlet Frequency Tiling

Glenn R. Easley[a,b], Vishal Patel[b], Dennis M. Healy, Jr.[b]

[a] System Planning Corporation, Arlington, Virginia
[b] University of Maryland, College Park, Maryland

## ABSTRACT

In this work, we present new methods for creating $M$-channel directional filters to construct multiresolution and multidirectional orthogonal/biorthogonal transforms. A key feature of these methods is the ability to solve the polynomial Bezout equation in higher dimensions by taking advantage of solutions that have been proposed for solving a related equation known as the *analytic Bezout equation*. These new techniques are capable of creating directional filters that yield spatial-frequency tilings equivalent to those of the contourlet and the shearlet transforms. Such directional filter banks can create sparse representations for a large class of images and can be used for various restoration problems, compression schemes, and image enhancements.

**Keywords:** directional filter, wavelet, shearlet, multichannel deconvolution.

## 1. INTRODUCTION

In recent years there has been considerable interest in obtaining directionally-oriented image decompositions. Many of these decompositions (e.g. curvelets[20] and contourlets[8]) have been obtained by reshaping or resampling of the data. By contrast, we propose an $M$-channel directional filter bank (DFB) construction technique that avoids these adjustments and allows the projection of the data directly onto the desired directionally-oriented basis.

It is well known that wavelets provide a good representation for a large class of signals and images. One of the greatest successes of wavelet theory has been its ability to provide a mathematical framework that explains why certain signals can be sparsely represented when filtered by a wavelet-based filter bank. For instance, from a continuous perspective, wavelets can be shown to sparsely represent one-dimensional signals that are smooth away from point discontinuities. Indeed, the best $N$-term wavelet expansion for this type of signal yields an approximation error whose rate of decay, as a function of $N$, is the best possible.

It is also known that for a certain class of images that can be represented as piecewise-smooth functions that are smooth away from a $C^2$ edge (that is, a composite of a $C^2$ function plus an indicator function of a set whose boundary is $C^2$), wavelets do not yield the best possible decay rate. For this reason, the need for the development of a new generation of wavelet representations that exhibit many directional orientations and shapes has emerged. Curvelets, contourlets, and shearlets[10] are the result of trying to create richer representations. These transforms are known to yield an essentially optimal approximation rate.

The key element to achieving these approximation rates is that the spatial-frequency tilings of these transforms have frame elements whose support width approximately equals the square of the support length and the number of orientations is dependent on the scale. Figure 1 shows the spatial-frequency tilings of the contourlet (equivalent to the curvelet transform's tiling) and the shearlet transform. Although these transforms achieve similar spatial-frequency tilings, their implementations are completely different. Indeed, the original motivation for the contourlet transform was to implement the finite discrete version of the curvelet transform using a DFB. To gain insight about the various implementations, let us consider the historical development of directional filtering.

---

G.R.E: E-mail: geasley@sysplan.com, V.P.: E-mail: pvishalm@umd.edu, D.M.H.: E-mail: dhealy@math.umd.edu

### 1.1. Directional Filter Bank

In 1992, Bamberger and Smith constructed a 2-dimensional directional filter bank that can be maximally decimated while achieving perfect reconstruction.[1] The total number of subbands coefficients is the same as that of the original image, and these coefficients can be used to reconstruct the original image without any errors (like aliasing, amplitude and phase distortions). The DFB splits $[-\pi, \pi)^2$ into an even number of wedge-shaped regions. Each wedge-shaped frequency band captures image details along orientations orthogonal to the subband direction. A $2M$-band DFB can be implemented by an $M$-level binary tree structure consisting of $M$ levels of a two-band system.

However, designing 2-dimensional filters with required passbands while achieving perfect reconstruction is not an easy task. In the original construction of the DFB, the two-channel filter banks used in the binary tree structure are diamond filter banks and the input image must be modulated. One of the drawbacks of the Bamberger DFB is that the use of modulation rearranges the data into a diamond support which introduces a severe spatial distortion into the subbands by shuffling the low and high frequency. Furthermore, it is not shift-invariant. Shift-invariance is very important in many image processing applications such as image denoising and pattern recognition. Finally, as the Bamberger DFB is a purely directional image decomposition, it lacks the ability to capture the details on low, medium and high frequencies.

### 1.2. The Contourlet Transform

Do and Vetterli simplified the construction of the DFB by using only two building blocks: a filter bank with fan filters and resampling operations. The key insight in this construction is that by appropriately resampling the image before and after a 2-dimensional filter, one can obtain a whole different set of subband geometries.

The contourlet construction is based on this simplified DFB combined with an improved Laplacian-pyramid transform. The result of this construction is a spatial-frequency tiling similar to that produced by the discrete curvelet transform. We summarize the contourlet transform algorithm below.

**Discrete Contourlet Transform Algorithm**

Let $f_a^0$ be the given $N \times N$ image. Set $N_0 = N$ and let $M_j$ be the number of directions for level $j$. For $j = 1, \ldots, L$, do the following:

1. Apply the Laplacian-pyramid scheme to decompose $f_a^{j-1}$ into a low-pass $N_{j-1}/2 \times N_{j-1}/2$ image $f_a^j$ and a high-pass $N_{j-1} \times N_{j-1}$ image $f_d^j$.
2. Apply a version of the Bamberger and Smith directional filter bank to $f_d^j$ to obtain $\{f_{d,k}^j\}_{k=1}^{M_j}$.

The contourlet coefficients are given by the collection $\{f_{d,k}^j\}_{k=1}^{M_j}$ for $j = 1, \ldots, L$.

### 1.3. The Shearlet Transform

Consider the two-dimensional affine system

$$\{\psi_{ast}(x) = |\det M_{as}|^{-\frac{1}{2}}\, \psi(M_{as}^{-1}x - t) : t \in \mathbb{R}^2\},$$

where

$$M_{as} = \begin{pmatrix} 1 & s \\ 0 & 1 \end{pmatrix} \begin{pmatrix} a & 0 \\ 0 & \sqrt{a} \end{pmatrix}$$

is a product of a shearing and anisotropic dilation matrix for $(a, s) \in \mathbb{R}^+ \times \mathbb{R}$. The generating functions $\psi$ are such that

$$\hat{\psi}(\xi) = \hat{\psi}(\xi_1, \xi_2) = \hat{\psi}_1(\xi_1)\, \hat{\psi}_2(\frac{\xi_2}{\xi_1}),$$

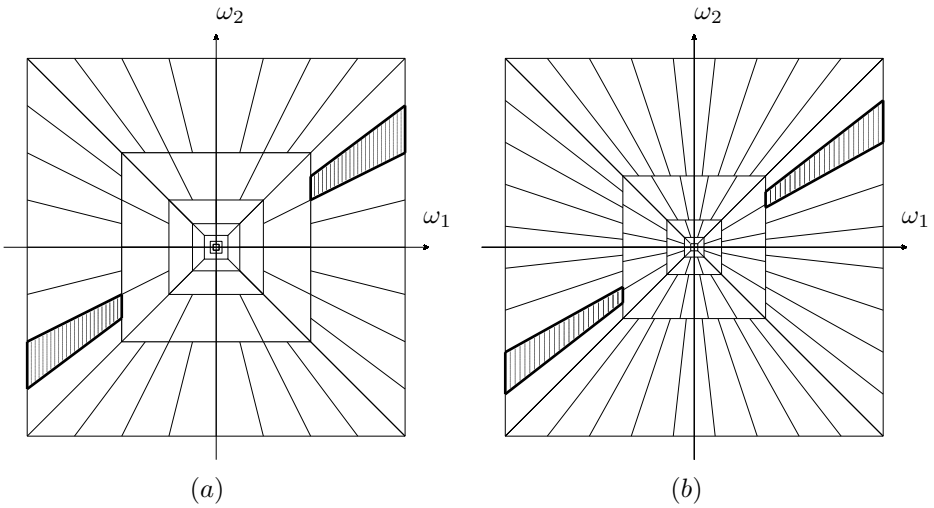


**Figure 1.** (a) The tiling of the frequency plane $\widehat{\mathbb{R}}$ induced by contourlets and curvelets. (b) The tiling of the frequency plane $\widehat{\mathbb{R}}$ induced by shearlets.

where $\psi_1$ is a continuous wavelet for which $\hat{\psi}_1 \in C^\infty(\mathbb{R})$ with $\operatorname{supp} \hat{\psi}_1 \subset [-2,-1/2] \cup [1/2,2]$, and $\psi_2$ is chosen so that $\|\psi_2\| = 1$, $\hat{\psi}_2 \in C^\infty(\mathbb{R})$, $\operatorname{supp} \hat{\psi}_2 \subset [-1,1]$, with $\hat{\psi}_2 > 0$ on $(-1,1)$. Then any $f \in L^2(\mathbb{R}^2)$ admits the representation

$$f(x) = \int_{\mathbb{R}^2} \int_{-\infty}^{\infty} \int_0^{\infty} \langle f, \psi_{ast} \rangle \, \psi_{ast}(x) \frac{da}{a^3} \, ds \, dt.$$

for $a \in \mathbb{R}^+$, $s \in \mathbb{R}$, and $t \in \mathbb{R}^2$. The operator $S$ defined by

$$Sf(a,s,t) = \langle f, \psi_{ast} \rangle$$

is called the *continuous shearlet transform* of $f \in L^2(\mathbb{R})$. It is dependent on the *scale* variable $a$, the *shear* $s$, and the *location* $t$.

The collection of *discrete shearlets* is described by

$$\{\psi_{j,\ell,k} = |\det A|^{j/2} \, \psi(B^\ell \, A^j x - k) : \, j, \ell \in \mathbb{Z}, k \in \mathbb{Z}^2\},$$

where

$$B = \begin{pmatrix} 1 & 1 \\ 0 & 1 \end{pmatrix}, \quad A = \begin{pmatrix} 2 & 0 \\ 0 & \sqrt{2} \end{pmatrix}.$$

A set of discrete shearlets that produce the frequency tiling shown in Figure 1 (b) can be described by combining shearlets supported on the horizontal cone $\mathcal{D}_0 = \{(\omega_1, \omega_2) \in \widehat{\mathbb{R}}^2 : \, |\omega_1| \geq \frac{1}{8}, |\frac{\omega_2}{\omega_1}| \leq 1\}$ and the vertical cone $\mathcal{D}_1 = \{(\omega_1, \omega_2) \in \widehat{\mathbb{R}}^2 : \, |\omega_2| \geq \frac{1}{8}, |\frac{\omega_1}{\omega_2}| \leq 1\}$.

The shearlet construction appears to be a natural extension of wavelets into two dimensions, but its implementation is not so natural partly because the filter constraints determined from a multiresolution analysis are not appropriate for filters that need to be implemented in a finite discrete domain. The algorithm of the shearlet transform is thus based on manipulating the data to obtain the desired spatial-frequency tiling determined by the theory. Define the pseudo-polar coordinates $(u,v) \in \mathbb{R}^2$ by

$$\begin{aligned} (u,v) &= \left(\omega_1, \frac{\omega_2}{\omega_1}\right) \quad \text{if } (\omega_1, \omega_2) \in \mathcal{D}_0, \\ (u,v) &= \left(\omega_2, \frac{\omega_1}{\omega_2}\right) \quad \text{if } (\omega_1, \omega_2) \in \mathcal{D}_1. \end{aligned}$$

The shearlet transform algorithm can be described as follows:

**Discrete Shearlet Transform Algorithm**

Let $f_a^0$ be the given $N \times N$ image. Set $N_0 = N$ and let $M_j$ be the number of directions for level $j$. For $j = 1, \ldots, L$, do the following:

1. Apply the Laplacian-pyramid scheme to decompose $f_a^{j-1}$ into a low-pass $N_{j-1}/4 \times N_{j-1}/4$ image $f_a^j$ and a high-pass $N_{j-1} \times N_{j-1}$ image $f_d^j$.
2. Compute $\widehat{f}_d^j$ on a pseudo-polar grid and apply filtering $\widehat{\psi}_{2,k}$ along the angular direction to obtain $\{\widehat{f}_{d,k}^j\}_{k=1}^{M_j}$.
3. Invert to obtain $\{f_{d,k}^j\}_{k=1}^{M}$.

The shearlet coefficients are given by the collection $\{f_{d,k}^j\}_{k=1}^{M_j}$ for $j = 1, \ldots, L$.

Although these tranforms share the goal of producing similar frequency tilings, the strategies to obtain these tilings are completely different. They each approach the problem by resampling the data either traditionally or by numerical and geometrical means. Most importantly, each step done separately in the algorithm is invertible.

It is possible to create analysis filters from these routines by applying them to an image representing a delta function. But it is not possible to create synthesis filters in a similar way. The clue to finding such filters is to look outside the field of filter design and to consider a special problem in the field of image restoration.

## 2. GENERAL APPROACH FOR M-CHANNEL DFB

In order to obtain an $M$-channel DFB and guarantee perfect reconstruction, we must design a set of analysis filters $\{H_i(\mathbf{z})\}_{i=0}^{m-1}$ and find synthesis filters $\{G_i(\mathbf{z})\}_{i=0}^{m-1}$ satisfying the Bezout polynomial equation

$$\sum_{i=0}^{m-1} G_i(\mathbf{z}) H_i(\mathbf{z}) = 1.$$

Notwithstanding the challenge of designing a pair of analysis filters in higher dimensions, in general the Bezout equation may not be solvable. In the cases when it is solvable, the standard algebraic techniques for solving the equation such as factorization are not applicable because no global factorization theorem exists. Thus, typical solutions rely on forming the higher-dimensional filters in a separable construction dependent on one-dimensional filter components.

In what follows, we provide a general DFB design that, when implemented for special cases, is essentially equivalent to the contourlet and shearlet transforms.

### 2.1. Analysis Filter Design

To create the analysis filters, we propose to follow a procedure similar to that of the nonsubsampled discrete shearlet transform. In this case, we propose using a family of scalar and wavelet functions $\varphi_1, \varphi_2, \psi_1$, and $\psi_2$ such that

$$|\widehat{\varphi}_1(\omega_t)\widehat{\varphi}_2(\omega_\theta)|^2 + \sum_{j \geq 0} \sum_{\ell=-2^j}^{2^j-1} |\hat{\psi}_1(2^{-j}\omega_t)\hat{\psi}_2(2^j\omega_\theta - \ell)|^2 = 1 \quad \text{for } (\omega_\theta, \omega_t) \in [0, 2\pi) \times [-1, 1].$$

Let $\phi_P$ be the mapping function from the Cartesian grid to the pseudo-polar grid and let $\hat{\psi}_{j,\ell}(\omega_\theta, \omega_t) = \hat{\psi}_1(2^{-j}\omega_t)\hat{\psi}_2(2^j\omega_\theta - \ell)$. The anaysis filters can then be formed as $\left(\phi_P^{-1}(\hat{\varphi}_1(\omega_t)\hat{\varphi}_2(\omega_\theta))\right)^\vee$ and $\left(\phi_P^{-1}(\hat{\psi}_{j,\ell}(\omega_\theta, \omega_t))\right)^\vee$ for $j \geq 0$ and $\ell = -2^j, \ldots, 2^j - 1$. For its implementation, we use a set of $m$ two-dimensional analysis filters that cover the psuedo-polar grid and invert the filters back into a Cartesian grid. Examples of a directional low-pass and high-pass filter found in this way are shown in Figure 3. Using this method, it is easy to create analysis

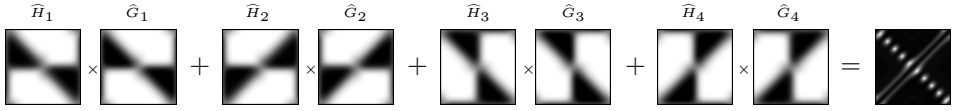


(a)

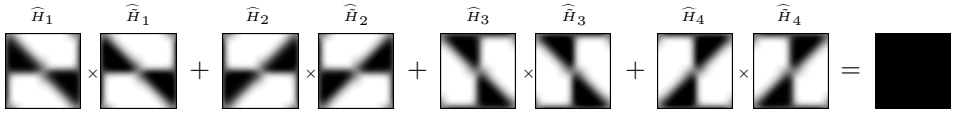


(b)

**Figure 2.** By applying the nonsubsampled contourlet transform to a delta function, we can obtain directional filters. (a) Failure of the perfect reconstruction condition using the analysis and synthesis filters found by applying the 2nd level decomposition to a delta function. (b) Using the analysis filters of (a) and the synthesis filters found through the MDP algorithm, perfection reconstruction is achieved.

filters that have the spatial-frequency tilings of the contourlet or shearlet transform. Figures 4 and 5 illustrate the result of convolving an image with analysis filters formed by this method.

Note that other types of mappings to create analysis filters that have more exotic spatial-frequency tilings could be used. We could also simply form the analysis filters by feeding a delta function image through various transforms. In general, these procedures are useless unless we can find the appropriate synthesis filters. Figure 2 (a) illustrates this point.

### 2.2. Synthesis Filter Design

In some applications of this design method, the synthesis filters are not easily constructed. To deal with this issue, we rely on recent advances in solving a related polynomial Bezout equation known as the Multichannel Deconvolution Problem (MDP).[2,3] In 1983 Berenstein and coauthors considered the following MDP: *Given a collection* $\{H_i\}_{i=1}^m$ *of compactly supported distributions on* $\mathbb{R}^d$ $(d \geq 2)$*, find a collection* $\{\tilde{H}_i\}_{i=1}^m$ *of compactly-supported distributions such that*

$$\sum_{i=0}^{m-1} \tilde{H}_i * H_i = \delta,$$

*where* $\delta$ *is a Dirac delta distribution.* In the Fourier-Laplace domain, this equation is known as the *analytic Bezout equation.* The methods for solving the MDP in a discrete setting provide a way of constructing appropriate synthesis filters (see [13], [12], [4], [22] for details on some of these methods).

As we have indicated above, the problem of finding reconstruction filters $G_i$ such that

$$\sum_{i=0}^{m-1} G_i * H_i = \delta$$

can be viewed as an $m$-channel deconvolution problem.

To the best of our knowledge, the idea of doing multichannel deconvolution in the field of micro-electroscopy was first conceived by P. Schiske in [17] and [18]. Schiske considered the problem of receiving more than one blurred image of an object produced from an electron microscope and the possibility of recovering the object's image from the received images. The underlying concept of his work was that if the transfer functions share no common zeros on the frequency domain, then the information lost in the received blurred image due to a frequency null of the transfer function could be recovered from the other blurred images. The problem from the Fourier transform axis is thus the following:

Suppose we wish to recover the image $f$ and that we are given $m$ blurred images $s_j$, i.e.

$$\widehat{s_j}(\boldsymbol{\omega}) = \widehat{f}(\boldsymbol{\omega})\widehat{H_j}(\boldsymbol{\omega}) + \widehat{n_j} \text{ for } j = 0, \ldots, m-1,$$

where $H_j$ and $n_j$ are the respective transfer function and associate noise from the $j$th imaging sensor. Assuming that no statistical information is available, find the image $f_a$ which yields a least squares fit between predicted and observed images, i.e., minimize

$$\sum_{j=0}^{m-1} |\widehat{s_j}(\boldsymbol{\omega}) - \widehat{f}_a(\boldsymbol{\omega})\widehat{H_j}(\boldsymbol{\omega})|^2.$$

After differentiating with respect to $\overline{\widehat{f}}_a$, the solution is found to be

$$\widehat{f}_a(\boldsymbol{\omega}) = \sum_{j=0}^{m-1} \widehat{s_j}(\boldsymbol{\omega})\widehat{G_j}(\boldsymbol{\omega})$$

where

$$\widehat{G_j}(\boldsymbol{\omega}) = \frac{\overline{\widehat{H_i}}(\boldsymbol{\omega})}{\sum_{k=0}^{m-1} |\widehat{H_k}(\boldsymbol{\omega})|^2},$$

for $j = 0, \ldots, m-1$,.

These synthesis filters are robust (and even optimal) with respect to any residual noise left from the directional decompositions that might remain after thresholding schemes have been utilized for denoising purposes. However, these solutions are not solutions to the MDP since they are not compactly-supported distributions or finite impulse response filters.[5]

For the implementation of our directional filter bank, Schiske's solutions become an issue if we restrict the type of convolution used. They are valid and useful when the convolutions are implemented making periodic boundary assumptions. For the purpose of our demonstrations, we shall use the synthesis filters found by using Schiske's solution. Our main interest in finding compactly-supported or finite duration reconstruction filters is more for computational efficiently than for greater flexibility in its implementation.

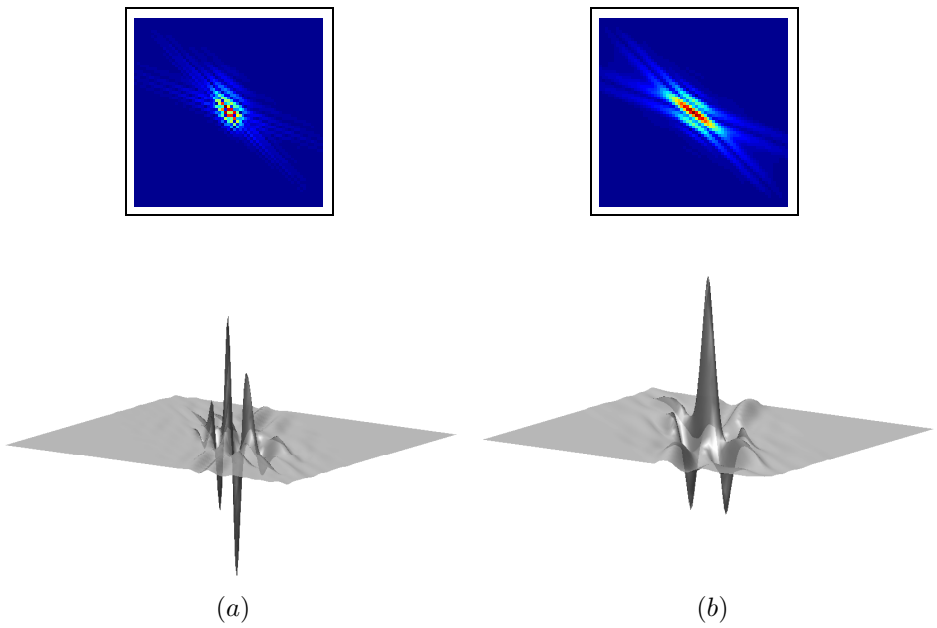

$(a)$ $(b)$

**Figure 3.** Images of directional filters. Figure (a) corresponds to a high-pass directional filter. Figure (b) corresponds to a low-pass directional filter.

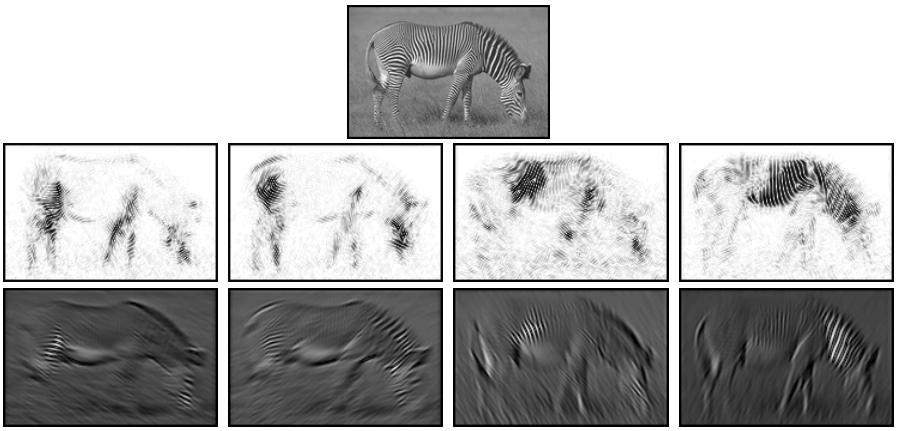

**Figure 4.** Directionally-filtered images of the "zebra" image. The top row corresponds to the high-pass directionally-filtered images (grayscale inverted for clarity). The bottom row corresponds to low-pass directionally-filtered images.

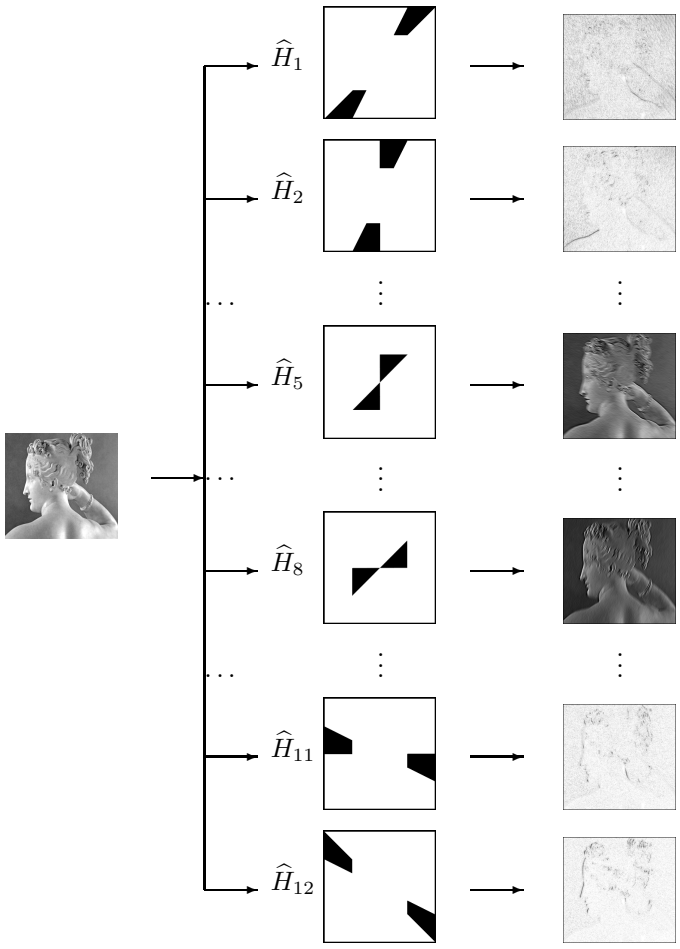


**Figure 5**. An illustration of the scheme for implementing the new $M$-channel directional filter bank design.

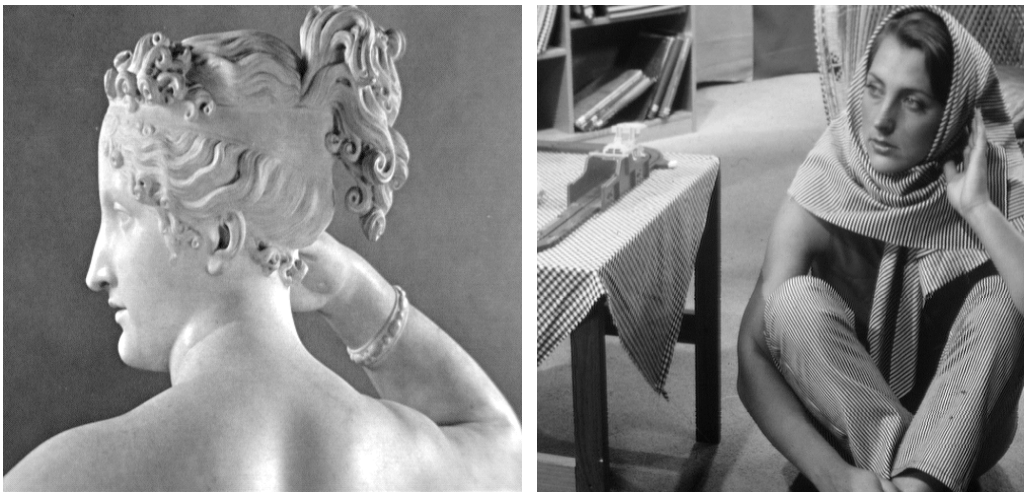

**Figure 6**. Test images: Paolina (left), Barbara (right).

## 3. EXPERIMENTAL RESULTS

To illustrate one of the uses of our $M$-channel DFB design, we tested its ability to remove noise from images. Specifically, suppose that corresponding to an image $f$, we are given

$$s = f + \epsilon \tag{1}$$

where $\epsilon$ is Gaussian white noise with zero mean and standard deviation $\sigma$. We attempt to recover $f$ from the noisy data $s$ by computing an approximation $\tilde{f}$ of $f$ obtained by applying a soft thresholding scheme in the subbands of the $M$-channel DFB similar to that given in [6]. More precisely, we use the DFB and choose the threshold parameters

$$\tau_{i,j} = \sigma^2_{\epsilon_{i,j}} / \sigma^2_{i,j,n} \tag{2}$$

where $\sigma^2_{i,j,n}$ is the variance of the $n$-th coefficient at the $i$th direction subband in the $j$th scale and $\sigma^2_{\epsilon_{i,j}}$ is the noise variance at scale $j$ and direction $i$. To estimate the signal variances in each subband locally, we use the neighboring coefficients contained in a square window and a maximum likelihood estimator. The variances $\sigma^2_{\epsilon_{i,j}}$, estimated by using a Monte-Carlo technique, are computed for several normalized noise images and the estimates are then averaged.

We tested the denoising method on the images of *Paolina* and *Barbara* shown in Figure 6 using an $M$-channel DFB that obtains the same spatial-frequency tiling of the contourlet transform.[6] For comparison, we tested the performance against a standard denoising routine of the discrete wavelet transform using the Daubechies-Antonini 7/9 filters (hard-thresholding was applied to the coefficients). In addition, we performed denoising based on the Bivariate Shrinkage algorithm using the Dual-tree Discrete Wavelet Transform (BivShrink)[19] and the curvelet denoising algorithm given in [20] .

## 4. CONCLUSION

We have developed a general scheme for creating an $M$-channel directional filter bank. The key component is the realization that the synthesis filters can be found by viewing the problem as a multichannel deconvolution problem. The algorithms and techniques developed to solve the MDP allow for the possibility of creating far greater variety in directional filtering than would be possible by standard analytical methods. One of the directional filter banks that we designed using this scheme showed better performance than many of the current competitive techniques. An advantage of an $M$-channel directional filter bank is that it can project the image directly onto the desired coefficient basis. Furthermore, this type of filter bank can be implemented in the order of $N^2 \log N$ operations for an $N \times N$ image. This technique provides an important tool for developing future filtering schemes.

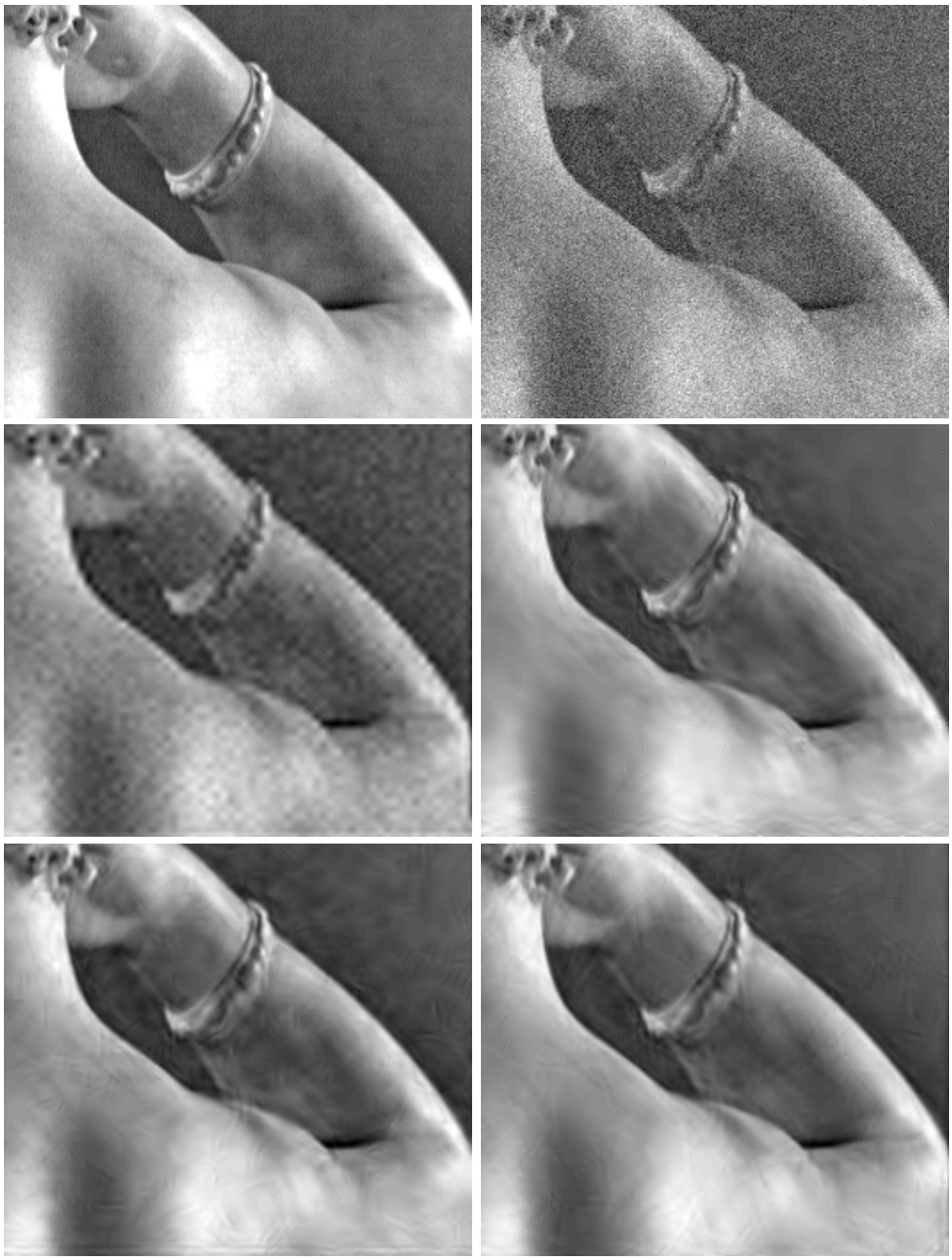

**Figure 7.** Close-up experimental results – From top left, clockwise: Original Image, Noisy image (PSNR= 22.12 dB), (BivShrink) using the Dual-tree Discrete Wavelet Transform (PSNR=32.30 dB), generalized Directional Filter Bank (PSNR= 32.52 dB), Curvelet Transform (PSNR= 31.85 dB), and Discrete Wavelet Transform defined in terms of the Daubechies-Antonini 7/9 filters (PSNR= 28.63 dB).

**Figure 8.** Close-up experimental results – From top left, clockwise: Original Image, Noisy image (PSNR= 22.12 dB), (BivShrink) using the Dual-tree Discrete Wavelet Transform (PSNR=29.72 dB), generalized Directional Filter Bank (PSNR= 29.97 dB), Curvelet Transform (PSNR= 26.58 dB), and Discrete Wavelet Transform defined in terms of the Daubechies-Antonini 7/9 filters (PSNR= 23.61 dB).

## REFERENCES


1. R. H. Bamberger, and M. J. T. Smith, "A filter bank for directional decomposition of images: theory and design", *IEEE Trans. Signal Proc.* **40**, pp. 882–893, 1992.
2. C. A. Berenstein, A. Yger, and B. A. Taylor, "Sur quelques formules explicites de deconvolution," *Journal of Optics (Paris)*, **14**, pp. 75–82, 1983.
3. C. A. Berenstein, and A. Yger, "Le problème de la déconvolution", *J. Funct. Anal.*, pp. 113–160, 1983.
4. F. Colonna, and G. R. Easley, "The multichannel deconvolution problem: a discrete analysis", *J. Fourier Anal. Appl.*, **10**, pp. 351–376, 2004.
5. F. Colonna, and G. R. Easley, "Generalized discrete Radon transforms and their use in the ridgelet transform," *Journal of Mathematical Imaging and Vision*, **23**, pp. 351–376, 2005.
6. A. L. Cunha, J. Zhou, and M. N. Do, "The nonsubsampled contourlet transform: Theory, design, and applications", *IEEE Trans. Image Proc.*, **15**, pp. 3089–3101, 2006.
7. M. N. Do, and M. Vetterli, "Image denoising using orthonormal finite ridgelet transform," *Proc. of SPIE Conference on Wavelet Applications in Signal and Image Processing VIII,* ***4119***, 2000.
8. M. N. Do, and M. Vetterli, "The contourlet transform: an efficient directional multiresolution image representation", *IEEE Trans. Image Proc.*, **14**, pp. 2091–2106, 2005.
9. G. R. Easley. *Computational solutions to the multi-channel deconvolution problem via the analytic Bezout equation.* Doctoral dissertation, George Mason University, 2000.
10. G. R. Easley, D. Labate, and W. Q Lim, "Optimally sparse image representations using shearlets", *Proc. 40th Asilomar Conf. on Signals, Systems, and Computers*, Monterey (2006).
11. G. R. Easley, D. Labate, and W. Q Lim, "Sparse Directional Image Representations using the Discrete Shearlet Transform", *preprint.*
12. G. R. Easley, and D. F. Walnut, "Local multichannel deconvolution," Journal of Mathematical Imaging and Vision, **18**, pp. 69-80, 2003.
13. G. Harikumar, and Y. Bresler, "FIR perfect signal reconstruction from multiple convolutions: minimum deconvolver orders", *IEEE Transactions on Signal Proc.*, **46**, pp. 215–218, 1998.
14. N. Kingsbury, "Complex wavelets for shift invariant analysis and filtering of signals", *Appl. Computat. Harmon. Anal.*, **10**, pp. 234-253, 2001.
15. J. H. McClellan, "The design of two-dimensional digital filters by transformation," *Proc. 7th Annual Priceton Conf. Information Sciences and Systems*, 1973.
16. E. Le Pennec, and S. Mallat, "Sparse geometric image representations with bandelets", *IEEE Trans. Image Proc.*, **14**, pp. 423–438, 2005.
17. P. Schiske, "Zur frage der bildrekonstruktion durch fokusreihen," *Proc. Eur. Reg. Conf. Electron. Microsc., 4th*, pp. 1–145, 1968.
18. P. Schiske, Image processing using additional statistical information about the object. In P. W. Hawkes, editor, *Image Processing and Computer Aided Design in Electron Optics.* Academic Press, New York, 1973.
19. L. Sendur, and I. W. Selesnick, "Bivariance shrinkage with local variance estimator", *IEEE Signal Proc. Letters*, **9**, pp. 438–441, 2002.
20. J. L. Starck, E. J. Candès, and D. L. Donoho, "The curvelet transform for image denoising", *IEEE Trans. Im. Proc.*, **11**, pp. 670-684, 2002.
21. D. F. Walnut, "Solutions to deconvolution equations using nonperiodic sampling," *J. Fourier Anal. Appl.*, **4**, pp. 669–709, 1998.
22. J. Zhou, and M. N. Do, "Multidimensional Multichannel FIR Deconvolution Using Gröbner Bases", *IEEE Trans. Image Proc.*, **15**, pp. 2998–3007 , 2006.